Effects of mesoscopic flow on ultrasonic velocities

Qiaomu Qi[a], T M. Müller [b], Boris Gurevich[a,b], Sofia Lopes[a] and Maxim Lebedev[a]

[a]Curtin University, Perth, Australia; [b]CSIRO, Perth, Australia.
Email: qiaomu.qi1@postgrad.curtin.edu.au

Summary

Mesoscopic flow is a significant mechanism of fluid-related seismic attenuation in partially saturated rocks. Attenuation due to this mechanism is controlled by spatial distribution of fluids. To study this effect in the laboratory we quantify mesoscale fluid distribution from CT scans and compute its associated acoustic signatures using poroelasticity theory. By comparing these theoretical estimates with experimentally measured velocities, we find that mesoscopic flow underestimates elastic wave attenuation at ultrasonic frequencies.

Introduction

Partial rock saturation can cause substantial dispersion and attenuation of P-waves due to mesoscopic flow of the pore fluid induced by the passing wave. A laboratory experimental setup suitable to study this mechanism is the simultaneous acquisition of X-ray tomography images and acoustic measurements during fluid injection. There have been several studies of this kind (Cadoret et al., 1995; Monsen and Johnstad 2005; Lebedev et al., 2009). Some of these studies reveal that attenuation and phase velocity are affected by fluid distribution which itself depends on the degree of saturation and saturation progress. However, variations in velocities and attenuation were related only qualitatively with simple saturation patterns (uniform, patchy) and no attempt was made to characterize fluid distribution in a quantitative way.

Toms et al., (2009) estimated P-wave dispersion and attenuation due to mesoscopic flow using the so-called continuous random medium (CRM) theory, which includes the influence of experimentally observed fluid distribution. However, due to lack of acoustic measurements, their wave attenuation estimates could not be corroborated.

The present work is based on laboratory study of Lopes and Lebedev (2012). In the experiment, simultaneous X-ray/acoustic data acquisition has been performed on a limestone sample. We aim to compare experimentally derived velocities against CRM theoretical estimates, which utilize geometric fluid distribution information extracted from the tomographic images. We examine whether mesoscopic fluid flow is the controlling factor on the acoustic properties of partially saturated rock at ultrasonic frequencies.

Experiment

The experimental setup is shown in Figure 1(a) and involves forced water imbibition into a Savonnieres limestone cylinder from its bottom. Ultrasonic measurements are conducted during water injection. By using broadband ultrasonic transducers, P- and S-waves propagating in the direction perpendicular to the core axis are recorded. P-wave waveforms are shown in Figure 1(b). Velocities are calculated by picking the first-break of the waveforms. Simultaneously, images of the core sample at various saturation stages are taken by a medical X-ray scanner. By implementing the processing procedure of Cadoret et al., (1995) on the raw CT scans, we construct the water-saturation maps; an example is displayed in Figure

1(c). The image's pixel color signifies percentage of water in the represented pore space. This time-space monitoring allows us to link P-wave velocity with its corresponding local saturation and mesoscopic saturation pattern.

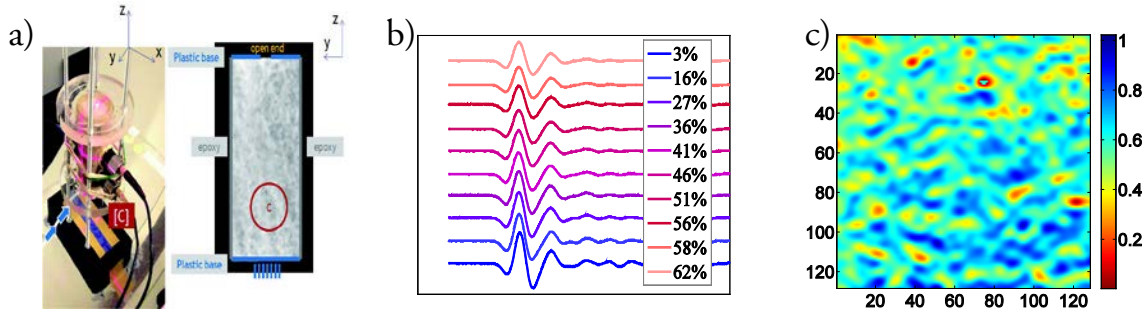

Figure 1. a) Experimental setup and raw CT scan, position C represents the acoustic monitoring area; b) Ultrasonic waveforms at various saturations; c) Water-saturation map at 58% water saturation of a square section cut at position C. Colorbar refers to saturation.

Statistical characterisation of fluid distribution

In order to characterize the fluid distribution, the global-threshold segmentation is applied to the water-saturation map using the pixels' mean distribution value. The image is idealised as a two phase medium consisting of water and gas while preserving most morphological features. The autocovariance functions are extracted from such images. In Figure 2(a), the normalized correlation functions for water saturation of 46% to 68% are plotted.

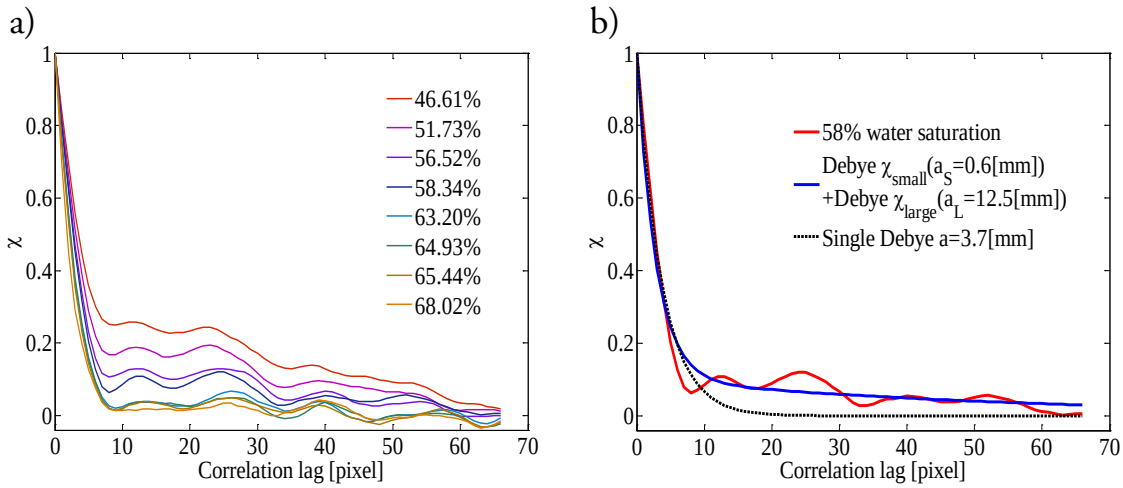

Figure 2. a) Normalized correlation functions at various water saturations; b) Comparison between two approximation methods

A useful way to characterise a binary medium is approximate the correlation function by an exponential Debye correlation function

$$\chi(r) = e^{-|r|/a_D}. \quad (1)$$

Where a_D is a characteristic length scale known as - Debye correlation length. Exponential correlation function leads to closed form solution of the dispersion equation for partially saturated media. It is indicated in Figure 2(b) that correlation function cannot be accurately approximated by a single Debye correlation function. In order to reflect the closest fluid distribution information, we employ a compound Debye function here. According to Figure 2(b), the fitting error is reduced from RMS 0.06 to 0.03 when utilizing the superposition model. The compound Debye correlation function is given by:

$$\chi_2(\mathrm{r}) = \chi_{\mathrm{small}} + \chi_{\mathrm{large}} = b_S e^{-|\mathrm{r}|/\mathrm{a_s}} + b_L e^{-|\mathrm{r}|/\mathrm{a_L}}, \quad (2)$$

where b_S and b_L are weighting coefficients with $b_S + b_L = 1$.

Modelling wave dispersion and attenuation

In the limiting cases of low and high wave frequencies, the uniform and patchy saturation bounds apply. Then the saturated P-wave modulus of each case can respectively be modelled through Gassmann-Wood (GW) and Gassmann-Hill (GH) theory. At intermediate wave frequencies or intermediate patch sizes (larger than the pore size, but smaller than the wavelength), uneven deformation of fluid patches by the passing wave results in mesoscopic fluid flow, which causes wave attenuation and velocity dispersion. In this physical picture, the acoustic signatures can be modelled by 3D continuous random model. The CRM theory assumes that the fluid distribution is quantified via a correlation function and thus enables us to compute velocity and quality factor due to real fluid distribution. According to the CRM model, the complex and frequency-dependent P-wave modulus can be expressed as:

$$\widetilde{H} = H^W(1 + \delta[\tau\xi^2 + (\tau - 1)\xi]). \tag{3}$$

The frequency dependence is contained in the function ξ

$$\xi(\omega) = k_{sP}^2 \int_0^\infty r B_M(r) e^{[ik_{sP}r]} dr, \tag{4}$$

where $B_M(r)$ is the normalized correlation function extracted from the fluid modulus map. By substituting equation (2) into equation (4), closed form of ξ can be expressed as

$$\xi(\omega) = b_S \frac{k_{sP}^2 a_S^2}{(ik_{sP}a_S - 1)^2} + b_L \frac{k_{sP}^2 a_L^2}{(ik_{sP}a_L - 1)^2}. \tag{5}$$

In equation (3) and (4), $k_{sP} = \sqrt{i\omega\eta/\kappa N}$ is the wavenumber of the Biot's slow P-wave, H^H, H^W are P-wave moduli corresponding to GH and GW limits, respectively. The scaling function $(H^H - H^W)/H^W$ ensures the convergence to the GH and GW bounds. The factor τ is given by:

$$\tau = \frac{\alpha N \sigma_{MM}^2}{4H}, \tag{6}$$

where Biot-Willis coefficient $\alpha = 1 - K_{dry}/K_s$, porelastic parameter N is given by $N = ML/H$, saturated and dry P-wave modulus H, L are related via $H = K_{sat} + 4/3\mu_{sat}$, $L = K_{dry} + 4/3\mu_{dry}$, where $\mu_{sat} = \mu_{dry}$. The saturated and dry bulk moduli are related via Gassmann equation $K_{sat} = K_{dry} + M_b\alpha^2$. The saturation weighted background fluid modulus is $M_b = M_1 v_1 + M_2 v_2$, where the fluid storage modulus of each phase is given by $M_i = ((\alpha - \phi)/K_s + \phi/K_i)^{-1}$, K_i is fluid bulk modulus of each phase, v_i is volume fraction of each phase, σ_{MM}^2 is normalized variance of the partitioned fluid modulus map. The petrophysical properties of the rock and fluids are specified in Table 1.

Table 1. Petrophysical properties of rock and fluids

Rock	$K_{dry}\ (GPa)^a$	$K_s\ (GPa)$	$\mu_{dry,sat}\ (GPa)^a$	$\rho_s\ (g/cm^3)$	$\kappa(mD)$	ϕ
Limestone	10.04	70	9.26	1.94	91	26.5%-28.5%
Fluids	$K_f\ (GPa)$		$\rho_f\ (g/cm^3)$		$\eta_f\ (Pa\ s)$	
Water	2.5		1.04		1e-3	
Gas	1e-4		1e-3		1e-5	

[a] K_{dry} and μ are computed using $K_{dry} = \rho_s V_p^2 - 4/3\mu$, $\mu = \rho_s V_s^2$, V_p, V_s are measured dry rock velocity

Comparison between experiment and theory

We compare the velocity-saturation relations (velocity saturation relation) deduced from the experiment with the predictions of the CRM model. Figure 3 indicates the experimental VSR and the VSR generated by the CRM model. Error bars for the experimentally derived velocities are used to account for errors in the travel time picking. Two percent of porosity variation is taken into consideration, as the limestone sample shows significant local porosity variations. This results in two sets of bounds and VSRs. In Figure 3, velocities obtained from the

experiment are larger than velocities predicted through CRM theory. The discrepancy between two velocities is averaged 61 (ϕ=28.5%) -80 (ϕ=26.5%)) m/s, 54% velocity departure behaviour from Gassmann-Wood bound can be attributed to the mesoscopic flow.

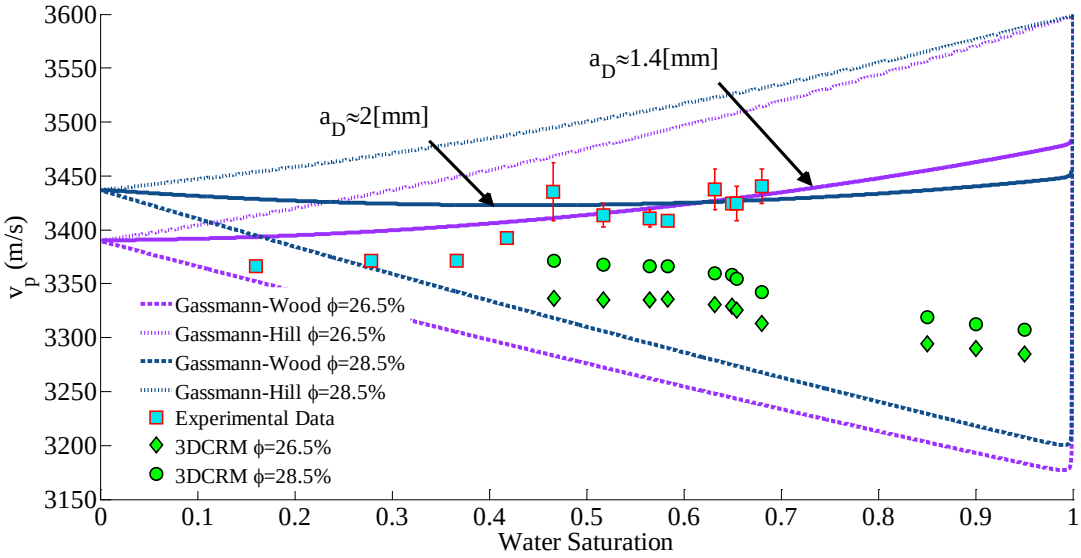

Figure 3. Comparison of VSR obtained from the experiment (cyan squares) and theory for porosity 28.5% (circles) and 26.5% (diamonds). The solid, dashed and dotted lines are the CRM predictions with constant correlation length, GW bounds, and GH bounds respectively

Conclusions

Though the analysis of the CT scans shows that there are mesoscale fluid patches, the mechanism of wave-induced flow between mesoscale patches is not able to fully explain the measured ultrasonic velocities. Larger fluid patches could explain the experimental data, however, no evidence of such larger patches has been found. This indicates that other mechanisms could contribute to the overall dynamic rock stiffening effect. Possible mechanisms include local flow between microscopic fluid patches and also the velocity dispersion associated with the transition from the viscosity- to the inertia-dominated wave-induced flow regime. In addition, capillary fingering can be significant at low injection rate, and in reservoir rocks of small pore diameter such as carbonates. Failing to account for capillary forces in the analysis of partially saturated rocks can lead to velocity underestimation. It is our further interest to cover this aspect.

Acknowledgements

This work was partially funded by Australia-China Natural Gas Technology Fund (Contract Number CTR-DJ-04194-1), CSIRO and Curtin Reservoir Geophysics Consortium.

References

Cadoret, T., D. Marion, and B. Zinszner. [1995] Influence of frequency and fluid distribution on elastic wave velocities in partially saturated limestones: *Journal of Geophysical Research*, **100**, 9789-9803.

Monsen, K., and S.E. Johnstad. [2005] Improved understanding of velocity-saturation relation-ships using 4D computer-tomography acoustic measurements: *Geophysical Prospecting*, **53**, pp. 173-181.

Lebedev, M., J. Toms-Stewart, B. Clennell, V. Shulakova, M. Pervukhina, L. Paterson, T.M. Müller, B. Gurevich, and F.Wenzlau. [2009] Direct laboratory observation of patchy saturation and its effects on ultrasonic velocities: *The Leading Edge*, **28**, 24-27.

Toms, J., T. M. Müller, B. Gurevich, and L. Paterson. [2009] Statistical characterization of gas-patch distributions in partially saturated rocks: *Geophysics*, **74**, no. 2, WA51-WA64